Neuron 52, 335–345, October 19, 2006 ©2006 Elsevier Inc. DOI 10.1016/j.neuron.2006.07.022

Sensory-Evoked Intrinsic Optical Signals in the Olfactory Bulb Are Coupled to Glutamate Release and Uptake

Hirac Gurden,[1,2] Naoshige Uchida,[1,3] and Zachary F. Mainen[1,*]
[1] Cold Spring Harbor Laboratory
1 Bungtown Road
Cold Spring Harbor, New York, 11724

Summary

Functional imaging signals arise from metabolic and hemodynamic activity, but how these processes are related to the synaptic and electrical activity of neurons is not well understood. To provide insight into this issue, we used in vivo imaging and simultaneous local pharmacology to study how sensory-evoked neural activity leads to intrinsic optical signals (IOS) in the well-defined circuitry of the olfactory glomerulus. Odor-evoked IOS were tightly coupled to release of glutamate and were strongly modulated by activation of presynaptic dopamine and GABA-B receptors. Surprisingly, IOS were independent of postsynaptic transmission through ionotropic or metabotropic glutamate receptors, but instead were inhibited when uptake by astrocytic glutamate transporters was blocked. These data suggest that presynaptic glutamate release and uptake by astrocytes form a critical pathway through which neural activity is linked to metabolic processing and hence to functional imaging signals.

Introduction

Functional imaging methods provide a readout of distributed patterns of brain activity that cannot be readily obtained with electrophysiological recordings. Intrinsic optical signals (IOS) have provided unique insight into the functional architecture of brain circuitry, notably those of the visual system (Bonhoeffer and Grinvald, 1991; 1996) and the olfactory bulb (Rubin and Katz 1999; Uchida et al., 2000; Meister and Bonhoeffer, 2001; Wachowiak and Cohen, 2003; Uchida and Mainen 2003). However, despite their utility, the relationship of functional imaging signals to conventional neural activity remains poorly understood (Bonvento et al., 2002; Heeger and Ress, 2002; Raichle, 2003). Functional signals are generally derived from metabolic and vascular responses to neural activity. In particular, changes in blood oxygenation and flow produce both IOS and fMRI signals (Ogawa et al., 1990; Bonhoeffer and Grinvald, 1996), while light-scattering changes related to metabolic activity also contribute to IOS (Aitken et al., 1999). Therefore, understanding how metabolism is coupled to electrical and synaptic activity would provide important insight into the interpretation of functional imaging signals (Shulman and Rothman, 1998; Magistretti et al., 1999; Raichle and Mintun, 2006).

Excitatory postsynaptic potentials and action potentials are predicted to be the most energetically costly components of neural signaling (Attwell and Laughlin, 2001), but energy supply and consumption in the brain are not passively coupled; rather, they are linked by active and dynamic processes (Attwell and Iadecola, 2002). Indeed, spiking activity can be completely decoupled from cerebral blood flow changes (Mathiesen et al., 1998; Caesar et al., 2003; Thomsen et al., 2004). The processes by which neurons signal their energy needs are not well understood, yet much evidence suggests that astrocytes are essential participants in the regulation of metabolic (Pellerin and Magistretti, 1994; Cholet et al., 2001; Voutsinos-Porche et al., 2003) and vascular responses (Zonta et al., 2003; Mulligan and MacVicar, 2004; Takano et al., 2005). Thus, it is possible that functional imaging signals depend more directly on activity in astrocytes than on activity in neurons. However, the involvement of astrocytes in functional imaging signals has never been demonstrated directly.

In this study, we used in vivo pharmacology, electrophysiology, and imaging to characterize the signaling pathways by which neural activity is linked to IOS in the olfactory bulb. Olfactory bulb IOS originate predominantly from the olfactory glomeruli (Meister and Bonhoeffer, 2001; Belluscio and Katz, 2001), spherical regions of neuropil with a relatively simple intrinsic circuitry that is advantageous for study of signaling pathways in vivo. Each glomerulus receives a unitary and homogeneous afferent input directly from a single type of primary sensory neuron (Wachowiak et al., 2004). Sensory afferents release glutamate onto local interneurons (juxtaglomerular cells; JGCs) and principal neurons (mitral and tufted cells; M/TCs), which form reciprocal synapses with one another and with presynaptic afferents (Shepherd and Greer, 1998).

We used local pharmacological manipulations to interfere with the pathway from odor-evoked action potentials in olfactory nerve inputs to the induction of IOS in the glomerulus. In this way, by probing the relative importance of presynaptic (release and astrocytic uptake) versus postsynaptic (activation of glutamate receptors) mechanisms in the genesis of the IOS, we could dissect the mechanisms of a functional imaging signal in vivo. We report two major results. First, the sensory-evoked IOS track presynaptic activity and are tightly regulated by dopamine (DA) and γ-amino-n-butyric acid (GABA)-B receptors. Second, the IOS are not dependent on postsynaptic glutamate receptor activation but are linked to glutamate release and uptake by astrocytic glutamate transporters.

Results

Activity Dependence of IOS Components

We imaged IOS in the dorsal olfactory bulb of anesthetized, freely breathing rats (Rubin and Katz, 1999;

*Correspondence: mainen@cshl.edu
[2] Present address: Laboratoire d'Imagerie et de Modélisation en Neurobiologie et Cancérologie CNRS UMR8165, Université Paris-Sud, 91406 Orsay Cedex, France.
[3] Present address: Center for Brain Science, Department of Molecular and Cellular Biology, Harvard University, 16 Divinity Avenue, Cambridge, Massachusetts 02138.

Uchida et al., 2000; Meister and Bonhoeffer, 2001). As previously reported, presentation of odors evoked large IOS. The odor-induced change in reflected light intensity (ΔR/R) often exceeded 1% and the signal-to-noise ratio was sufficient to resolve responses in single trials (Figure 1A). The raw odor-evoked ΔR/R signal could be decomposed into three components with different spatial characteristics. The first component (not shown) was a large-amplitude, low-frequency oscillation present in the absence of sensory stimuli (Meister and Bonhoeffer, 2001). The frequency range of this signal (0.1 to 0.15 Hz) matched descriptions of a vasomotion signal previously observed throughout the brain (Mayhew et al., 1996; Kleinfeld et al., 1998). Because this stimulus-independent component was spatially uniform, it was effectively removed by subtracting the spatial average over the entire image at each time point (see Experimental Procedures).

The remaining signals were time-locked to stimulus onset and showed odor-specific spatial patterns of increased absorption (darkening) (Rubin and Katz, 1999) (Figure 1B). These odor-induced IOS could be further separated by spatial filtering into low ($\Delta R/R_{lp}$) and high ($\Delta R/R_{hp}$) spatial frequency components, both of which remained time-locked to odor onset and showed odor-specific spatial distributions. High-pass filtered images (200 μm Gaussian smoothing kernel) showed a characteristic pattern of punctate spots approximately 50–150 μm in diameter, the pattern of which changed with odor identity.

By applying pharmacological agents concomitantly with optical imaging, we sought to dissect the pathway from neural activity to IOS. The amplitude of IOS evoked by the odor phenol (0.2%–0.4% of saturated vapor) was used to quantify drug effects because it evoked a restricted set of particularly discrete and bilaterally symmetric glomerular IOS. Drug effects were confirmed using structurally dissimilar odors (caproic acid and acetophenone) that evoked activity in other regions of the bulb.

We first used tetrodotoxin (TTX) to determine the components of the IOS that were dependent on neural activity. Direct injection of TTX (20–100 μM) through a micropipette produced a rapid local inhibition of both the punctate and the diffuse odor-evoked components of the IOS (n = 4). In contrast, TTX did not affect the slow oscillatory component (not shown). This result indicates that, as expected, the odor-evoked components of the IOS are indeed dependent on local neural activity in the form of action potentials. On the other hand, the putative vasomotion signal is not dependent on local spiking activity. Signals obtained using high-pass spatial filtering have been previously shown to have a high spatial correlation with histologically-defined glomeruli (Meister and Bonhoeffer, 2001). In the following experiments, unless otherwise noted, we based our measurements of IOS amplitude on the punctate component (high-pass filtered, $\Delta R/R_{hp}$ signal).

Although the pressure injection method was effective, in order to minimize trauma to the preparation, we used topical application of pharmacological agents in Gelfoam to the surface of the bulb (see Experimental Procedures). We used TTX to estimate the effective dilution of drugs produced by this method. In olfactory bulb slice preparations, TTX is effective at around 0.3 μM (Aroniadou-Anderjaska et al., 1999; Schoppa and Westbrook, 2001). Application of 1 μM TTX using Gelfoam was

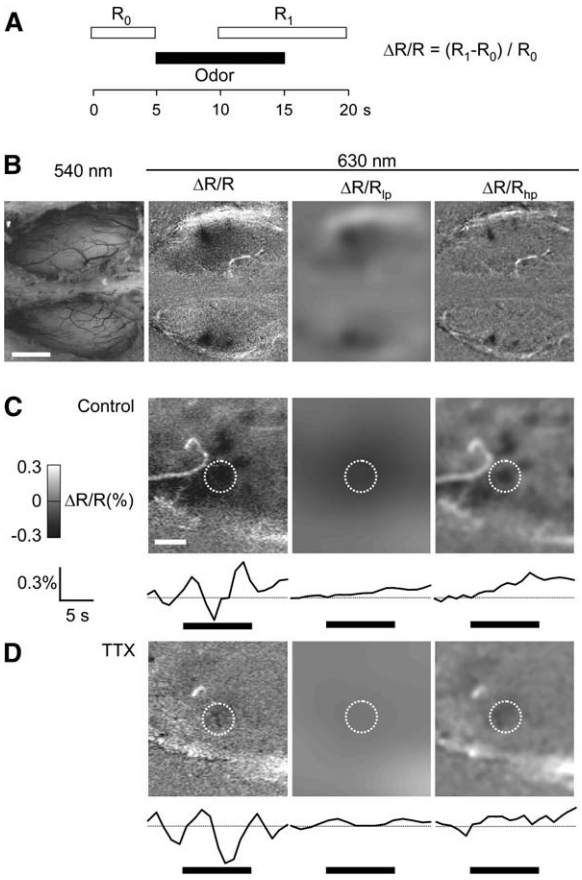

Figure 1. Description of Odor-Evoked IOS in the Olfactory Bulb

(A) Imaging protocol. IOS are recorded in a series of individual trials of 20 s duration. Diagram shows the timing of baseline (R_0) and response (R_1) images and the odor stimulus (black bar). Frames were acquired at 30 frames/s and R_0 and R_1 were calculated by averaging all frames in the time periods indicated.

(B) From left to right: The dorsal olfactory bulb illuminated at 540 nm. Raw ΔR/R image (average of five trials) at 630 nm evoked by phenol (0.2% of saturated vapor). Low-pass filtered image ($\Delta R/R_{lp}$; Gaussian kernel of σ = 200 μm). High-pass filtered image ($\Delta R/R_{hp}$). Note that the mean image value has been subtracted from both low-pass and high-pass filtered images. See Experimental Procedures for description of the decomposition of the raw image into components. In all images both left and right bulbs are shown and the antero-posterior axis is from left to right. Scale bar in the leftmost image shows 1 mm. The ΔR/R activity scale is shown in (C).

(C and D) Activity dependence of odor-evoked IOS components. A smaller region of one hemi-bulb is shown for the same image components as described in (B) (i.e., all images in a column were calculated in the same manner). The orientation and ΔR/R scale are the same as in (B). The spatial scale bar is 200 μm. (C) Control ΔR/R images in response to phenol. (D) ΔR/R images in response to phenol, taken after application of TTX (30 μM). The white dotted circle indicates a region of interest placed over the region responding to phenol. ΔR/R (raw, low-pass, or high-pass) from the region of interest was averaged and plotted at a resolution of 1 s to produce the time courses shown below each corresponding image. Note that the mean image value at each time point has been subtracted from both low-pass and high-pass filtered signals. Black bars on the time course graphs show the period of odor presentation. The thin horizontal line represents ΔR/R = 0.

without effect (96% ± 12% of control, n = 2), presumably due to the continual turnover of cerebrospinal fluid. A 30-fold higher concentration of TTX (30 μM), produced a nearly complete block of both punctate and diffuse odor-evoked signals (respectively, 5% ± 4% and 15% ± 8% of control; n = 2) (Figures 1C and 1D). From these data we estimated that in our experimental conditions the effective dilution was a factor of 50–100 compared to in vitro conditions. For further experiments we applied drugs at 500–1000 times the in vitro dosage in order to ensure effective concentrations were reached.

Presynaptic Regulation

Are IOS directly coupled to action potentials of afferent olfactory receptor neurons (ORNs) or do they require neurotransmitter release? In vitro studies show that DA D2 agonists (Coronas et al., 1997; Duchamp-Viret et al., 1997) and GABA-B agonists (Bonino et al., 1999; Koster et al., 1999; Duchamp-Viret et al., 2000) are capable of inhibiting electrically-evoked synaptic transmission from ORNs to M/TCs without affecting input action potentials (Nickell et al., 1994; Hsia et al., 1999; Wachowiak and Cohen, 1999; Aroniadou-Anderjaska et al., 2000; Berkowicz and Trombley, 2000; Ennis et al., 2001; Palouzier-Paulignan et al., 2002). These drugs mimic the action of DA and GABA release from JGCs by activating D2 and GABA-B receptors located on ORN terminals (McLean and Shipley, 1988; Coronas et al., 1997; Duchamp-Viret et al., 1997, 2000; Bonino et al., 1999; Koster et al., 1999; Gutierrez-Mecinas et al., 2005) and suppressing presynaptic Ca^{2+} influx and glutamate release (Hsia et al., 1999; Ennis et al., 2001; Wachowiak et al., 2005). Therefore, if IOS require neurotransmitter release, they should be sensitive to D2 and GABA-B agonists (see Figure 5 for a schematic representation of the glomerular network).

Coapplication of DA and GABA-B agonists (50 mM apomorphine and 10 mM baclofen) dramatically decreased odor-evoked IOS (Figure 2). In order to insure that possible rundown of IOS (Meister and Bonhoeffer, 2001) was not mistaken for agonist effects, we imaged left and right bulbs simultaneously and infused one bulb with drugs while the other bulb served as a control. DA and GABA-B agonist application reduced the signal in the treated bulb, while the signal in the control bulb was unaffected (Figures 2A and 2B). Figure 2C shows the trial-by-trial amplitude of odor-evoked responses over the course of this experiment. To obtain a population measurement, time courses from individual experiments were normalized to their average baseline amplitude and then averaged (Figure 2D). In the experiment shown in Figure 2C, both treated and control hemi-bulbs were stable throughout the baseline and treatment periods, but sometimes a small amount of rundown was seen. To control for this, reported drug effects (Figure 2E) were cross-normalized (i.e., the average normalized amplitude of the treated hemi-bulb was divided by the average normalized amplitude of the control hemi-bulb) (see Experimental Procedures).

In order to determine the relative contributions and possible interaction of DA and GABA-B receptors (Gall et al., 1987), we examined the effects of DA and GABA-B agonists separately. Apomorphine (50 mM) caused a significant reduction in IOS (70% ± 12% of control, $p < 0.05$, n = 3; Figure 2E), as did baclofen (10 mM) (66% ± 6% of control, $p < 0.05$, n = 3; Figure 2E). The combined DA and GABA-B agonists (50 mM apomorphine and 10 mM baclofen) produced a net (cross-normalized) reduction of the signal to 25% ± 12% of control ($p < 0.001$, n = 4; Figure 2E). The effectiveness of this combination in suppressing IOS (block almost equal to TTX) indicates that presynaptic action potentials are ineffective in generating IOS, unless they are coupled through some signaling pathway downstream of Ca^{2+} entry and transmitter release. The effect of the coapplied agonists was slightly greater than linear summation (75% block coapplied versus 30% + 34% = 64% block for the sum of individual effects). This result is consistent with the idea that DA and GABA systems act on distinct targets and indicates that both are effective in regulating glomerular metabolic activity as well as neural activity (Sallaz and Jourdan, 1992; Keller et al., 1998).

These experiments with exogenous agonists establish the potential capacity of DA and GABA-B receptors to suppress odor-evoked IOS, but does natural odor stimulation itself recruit such feedback inhibition? In vitro studies have found that GABA-B antagonists increased M/TCs activity evoked by electrical olfactory nerve stimulation (Aroniadou-Anderjaska et al., 2000). In vivo, imaging studies have recently shown an increase in odor-evoked presynaptic Ca^{2+} signals in the presence of GABA-B antagonists (Wachowiak et al., 2005; Vucinic et al., 2006). Block of GABA-B receptors by the specific GABA-B receptor antagonist 2S-(+)-5,5-dimethyl-2-morpholineacetic acid (SCH-50911) caused an increase in IOS (121% ± 12% of control, $p < 0.05$; n = 4). The strength of enhancement by GABA-B blockade was substantial relative to the reduction by baclofen injection (21% increase versus 34% decrease). This observation shows that sensory-evoked IOS are indeed modulated by endogenous as well as exogenous GABA-B receptor activation.

Postsynaptic Receptors

How is presynaptic activity linked to the generation of IOS? Postsynaptic ionotropic glutamate receptors (α-amino-3-hydroxy-5-methyl-4-isoxazolepropionic acid [AMPA] and *N*-methyl-D-aspartic acid [NMDA] receptors) are the major targets of glutamate released in glomeruli (Berkowicz et al., 1994; Ennis et al., 1996; Aroniadou-Anderjaska et al., 1997). Activation of these receptors creates postsynaptic potentials and action potentials in M/TCs and JGCs. Such postsynaptic activity has been proposed to be the major energy sink in the brain (Attwell and Laughlin, 2001) and has been suggested to underlie the generation of IOS (Bonhoeffer and Grinvald, 1996).

To test the contribution of postsynaptic sources to IOS, we applied a mixture of glutamate receptor antagonists—the NMDA receptor antagonist DL-2-amino-5-phosphonopentanoic acid (DL-APV) (50 mM) and the AMPA receptor antagonist 2,3-dioxo-6-nitro-1,2,3,4-tetrahydrobenzoquinoxaline-7-sulfonamide (NBQX) (5 mM). Surprisingly, this treatment caused no decrease in the IOS. An individual experiment is shown in Figures 3A–3C, and population data are shown in Figure 3D. The net effect of these antagonists was a small but

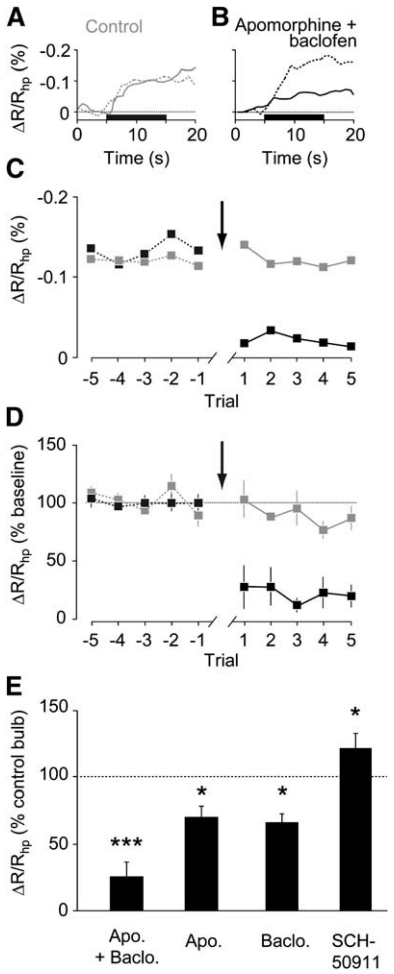

Figure 2. DA and GABA-B Receptor Agonists Block IOS

(A and B) An individual experiment showing the effect of a combination of DA and GABA-B agonists (apomorphine, 50 mM, and baclofen, 10 mM). The time course of the phenol-evoked IOS (high-pass filtered, $\Delta R/R_{hp}$) is shown for the control hemi-bulb (A) and the drug-treated hemi-bulb (B). Dashed line, baseline condition; solid line, same region after application of drug. Each trace is the average of three trials. Black bar indicates the period of odor presentation. IOS time courses were calculated using bilaterally symmetric regions of interest as described in Figure 1 and the Experimental Procedures.

(C) Trial-by-trial amplitude of IOS ($\Delta R/R_{hp}$) from the same experiment shown in (A) and (B). Gray symbols, control hemi-bulb; black symbols, treated hemi-bulb. Amplitudes were averaged over the time windows shown in Figure 1A. Arrow indicates the time of drug application.

(D) Population data showing average trial-by-trial amplitude of IOS for experiments like that depicted in (A–C) in which DA and GABA-B agonists were coapplied. The data were self-normalized by dividing by the average of baseline trials. Gray symbols, control hemi-bulb; black symbols, treated hemi-bulb. Each data point is the mean ± SEM (n = 4 animals).

(E) Summary of different experiments with DA and GABA-B agonists and antagonists. The value of the self-normalized amplitude in the treated hemi-bulb after drug application (averaged over 4–6 trials) was divided by the self-normalized amplitude in the corresponding control hemi-bulb over the same period. Bar graph shows, from left to right, DA and GABA-B agonists together (apomorphine, 50 mM, and baclofen, 10 mM, n = 4), DA agonist alone (apomorphine, 50 mM, n = 3), GABA-B agonist (baclofen, 10 mM, n = 3), and GABA-B antagonist (SCH-50911, 100 mM, n = 4). Error bars represent SEM across animals. Significance was calculated using a paired t test comparing self-normalized values of control and treated sides for each drug treatment (*$p < 0.05$; ***$p < 0.001$).

significant enhancement of the punctate glomerular signal (120% ± 4% of control, $p < 0.01$, n = 7; see Figure S1 in the Supplemental Data). This finding indicates that postsynaptic activation through fast synaptic signaling and consequent postsynaptic depolarization are not necessary for generation of odor-evoked IOS. A likely explanation for the increase in the odor-evoked signal is a blockade of AMPA/NMDA receptors on juxtaglomerular cells that normally provide feedback inhibition through GABA-B receptors (Wachowiak et al., 2005; McGann et al., 2005; Vucinic et al., 2006). The similar magnitudes of increase observed with the GABA-B antagonist SCH-50911 and NBQX/DL-APV suggest that blockade of presynaptic inhibition can fully account for the NBQX/DL-APV effect, but also that relief of inhibition is not large enough to mask a suppressive effect of NBQX/DL-APV. Interestingly, the odor-specific diffuse signal was typically enhanced to a greater extent than the punctate signal (139% ± 17% of control, $p < 0.05$, n = 7; Figure S1), consistent with a role for juxtaglomerular cells in interglomerular lateral inhibition (Vucinic et al., 2006).

To further establish that glutamate receptor antagonists were sufficient to block postsynaptic ionotropic glutamate responses, we tested the effect of DL-APV and NBQX on glomerular local field potentials (LFPs). Odor-evoked LFPs were oscillatory, variable in amplitude, and outlasted stimulation by many seconds. Therefore, we used electrical stimulation of the olfactory nerve to assay the effectiveness of glutamate antagonists. Electrically evoked LFPs recorded in the glomerular layer had temporal profiles similar to those previously described, acquired using olfactory nerve stimulation in slices (Aroniadou-Anderjaska et al., 1997), with an initial large negative deflection with a peak latency of 8.63 ± 0.13 ms (n = 4, Figure 3E). Application of NBQX (5 mM) + DL-APV (50 mM) topically to the bulb reduced LFP amplitude to 11% of control (−1.2 ± 0.2 mV baseline, −0.13 ± 0.03 mV in the presence of the antagonists, $p < 0.05$; n = 3). LFPs were stable under similar conditions in the absence of antagonists. We therefore conclude that glutamate receptor antagonists reach concentrations sufficient to block excitatory synaptic transmission and that activation of postsynaptic glutamate receptors is not required to generate odor-evoked IOS.

These experiments argue against a dependence of IOS on postsynaptic ionotropic glutamate receptors, but do not exclude the possibility of a metabotropic glutamate receptor (mGluR)-mediated pathway. Indeed, mGluR1 has been implicated in postsynaptic M/TC responses in vitro (Schoppa and Westbrook, 2001; Heinbockel et al., 2004; De Saint Jan and Westbrook, 2005; Yuan and Knopfel, 2006; Ennis et al., 2006). We checked for the involvement of mGluRs using the broad-spectrum group I/II antagonist (S)-α-methyl-4-carboxyphenylglycine (MCPG) (50 mM) and the more specific mGluR1 antagonist LY367385 (15 mM). Neither drug had an effect on the amplitude of odor-evoked IOS (MCPG: 99% ± 17% of control, n = 2, not shown; LY367385: 104% ± 9%, $p > 0.05$, n = 5, Figure 4E). Thus, neither ionotropic nor metabotropic postsynaptic glutamate receptors appear to mediate the coupling of neural activity to IOS.

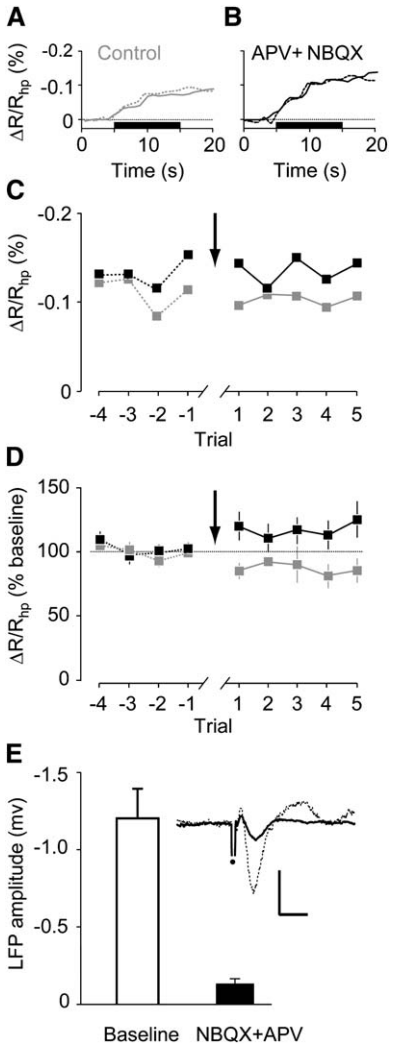

Figure 3. Glutamate Receptor Antagonists Fail to Block Odor-Evoked IOS

(A–D) The effect of glutamate receptor (AMPA and NMDA) antagonists (NBQX, 5 mM, and DL-APV, 50 mM) on the IOS. (A–C) Single experiment. (D) Population data (n = 4 animals). Calculations and symbols in (A–D) are as described in Figures 2A–2D.

(E) Bar graph shows LFP amplitude recorded in the glomerular layer in response to electrical ON-stimulation in vivo in control conditions and during application of NBQX and DL-APV (mean ± SEM, n = 3 animals). Inset shows average LFP traces from one experiment. Dotted trace, baseline condition, average of ten responses. Solid trace, application of NBQX (5 mM) + DL-APV (50 mM), average of 20 responses. Horizontal bar, 0.4 mV; vertical bar, 5 ms. The stimulus artifact (black dot) has been truncated.

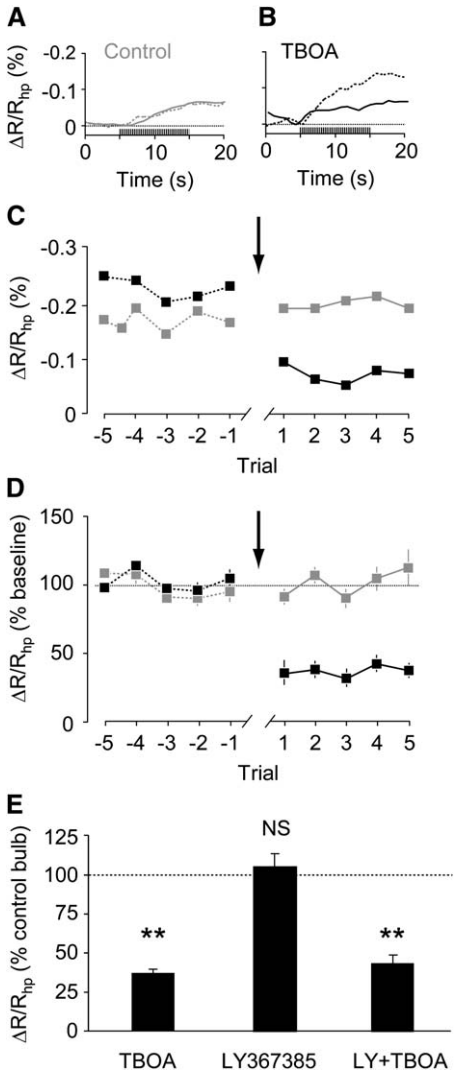

Figure 4. Glutamate Uptake Blocker TBOA Blocks IOS

(A–D) The effect of TBOA (10 mM), a blocker of the glutamate transporters GLT1 and GLAST, on the IOS. (A–C) Single experiment. (D) Population data (n = 5 animals). Calculations and symbols in (A–D) are as described for Figures 2A–2D.

(E) Summary of experiments with the glutamate transporter blocker TBOA and the metabotropic glutamate receptor antagonist LY367385. Bar graph shows, from left to right, effects of TBOA alone (n = 5), LY367385 alone (n = 5), and TBOA and LY367385 together (n = 4). Calculations are as describe for Figure 2E. (Statistical significance: NS, not significant, $p > 0.05$; **$p < 0.01$).

Glutamate Uptake

If IOS are downstream of presynaptic ORN activity, but independent of postsynaptic glutamate receptor activation, how is neural activity coupled to IOS? In addition to presynaptic and postsynaptic neuronal components, astrocytes are another arm of the synaptic signaling triad (Araque et al., 2001). Astrocytes are recognized as the central mediator of a host of critical metabolic and hemodynamic processes (Bonvento et al., 2002; Nedergaard et al., 2003). Glomeruli express low levels of neuronal glutamate transporters, but very high levels of the astrocytic glutamate transporters GLAST and GLT1, with GLAST dominating the core of the glomerulus and GLT1 dominating the surrounding shell (Utsumi et al., 2001). Both astrocytic transporters are responsible for glutamate clearance in olfactory glomeruli (De Saint Jan and Westbrook, 2005). In addition, glutamate uptake by astrocytes has been linked to the generation of IOS in vitro (Schneider et al., 1992; Buchheim et al., 2005). Could neural activity be linked to glomerular IOS through astrocytic glutamate uptake?

To test the role of astrocytic glutamate uptake in the generation of sensory-evoked IOS, we applied DL-threo-β-benzyloxyaspartate (TBOA), a very effective blocker of both GLAST and GLT1 (Figure 4) (De Saint

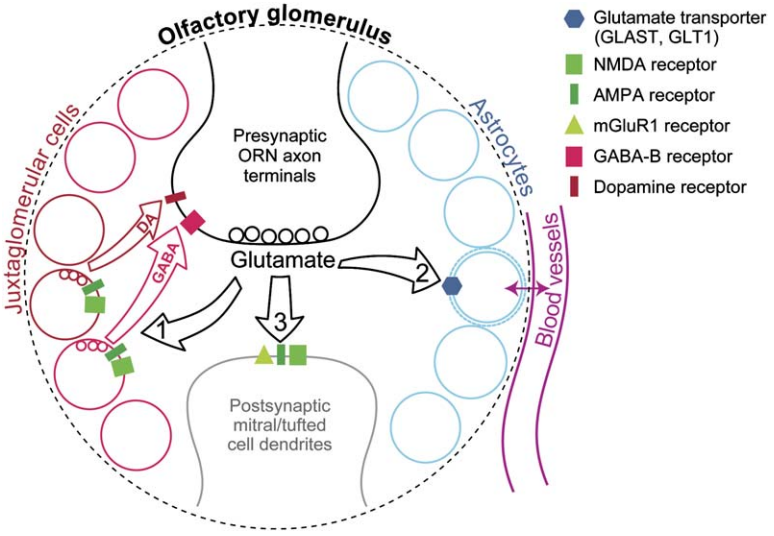

Figure 5. Circuitry of the Olfactory Glomerulus and Origins of Functional Optical Signals

Diagram illustrating the circuitry of the olfactory bulb glomerulus and proposed mechanisms underlying the generation of odor-evoked IOS. Glutamate released by sensory activation of ORNs acts via three pathways: (1) Juxtaglomerular cells, sensing glutamate by ionotropic receptors (AMPA and NMDA), provide inhibitory feedback control of release through dopamine (DA) and GABA acting on presynaptic receptors. (2) Astrocytes, activated by glutamate transporters (GLT1, GLAST), produce changes in light scattering (due to cell swelling) and blood flow, resulting in intrinsic optical signals (IOS). (3) Postsynaptic neurons, activated by metabotropic and ionotropic glutamate receptors, transmit electrical signals downstream but are independent of the generation of IOS.

Jan and Westbrook, 2005). Application of TBOA (10 mM) strongly inhibited odor-evoked IOS (Figures 4A and 4B). The time course of an individual experiment is shown in Figure 4C, and population data is shown in Figure 4D. The net (cross-normalized) amplitude of IOS in TBOA was reduced by about two-thirds (36% ± 6% of control, $p < 0.005$; $n = 5$).

The dependence of IOS on TBOA suggests that activation of astrocytic glutamate transporters could be a critical step in the pathway linking the sensory-evoked neuronal activity to IOS in the olfactory bulb. However, blockade of uptake enhances the concentration of glutamate in the glomerulus, which could recruit mGluR responses. TBOA (10 mM) applied topically to the olfactory bulb surface had a variable effect on electrically-evoked LFPs (39% ± 20% of control, $p > 0.05$; $n = 3$). TBOA is known to enhance mGluR1-mediated responses in M/TCs (De Saint Jan and Westbrook, 2005; Ennis et al., 2006; Yuan and Knopfel, 2006). In order to test whether TBOA acts by enhancing mGluR1 activity, we coapplied the mGluR1 antagonist LY367385 with TBOA. The block of IOS in the presence of the LY367385 was similar compared to TBOA alone (42% ± 6%, $n = 4$, $p < 0.01$; Figure 4E). Thus, we conclude that mGluR1 signaling does not mediate the inhibitory effects of TBOA.

Discussion

We used local pharmacology during in vivo imaging and electrophysiology to dissect the link between sensory-evoked neural activity and functional imaging signals. We found that odor-evoked IOS in the olfactory bulb are downstream of presynaptic glutamate release but do not depend on postsynaptic activity through either ionotropic or metabotropic glutamate receptors. IOS were blocked by an inhibitor of astrocytic glutamate uptake. Thus, glutamate release could be coupled to IOS directly through the activation of astrocytic glutamate transporters, although we did not rule out a contribution from other pathways. A schematic summarizing the inferred pathways is shown in Figure 5. Together, our data are consistent with the view that astrocytes play a critical role in coupling metabolic and vascular responses to neural activity and are hence essential to the genesis of functional imaging signals.

Coupling of IOS to Presynaptic, but Not Postsynaptic, Activity

We focused our analysis on a component of IOS that was time-locked to odor presentation and showed odor-specific patterns of punctate spots (Rubin and Katz 1999; Uchida et al., 2000; Wachowiak and Cohen, 2003; Uchida and Mainen 2003) previously shown to be correlated with anatomical markers of glomeruli (Meister and Bonhoeffer, 2001). Odor-specific IOS were completely blocked by TTX, demonstrating that they depend on action potentials. In addition, we found large IOS in the olfactory bulb in the form of an ongoing oscillatory (approximately 0.1 Hz) signal that was neither spatially nor temporally related to odor stimulation, nor sensitive to application of TTX. The frequency of this component suggests a correspondence with a previously described vasomotion signal (Mayhew et al., 1996; Kleinfeld et al., 1998) as opposed to an artifact of respiration (0.5–2 Hz) or heartbeat (3–8 Hz).

Sensory-evoked IOS were strongly inhibited by GABA-B and DA agonists. In vitro studies have shown that the same agonists are capable of suppressing synaptic potentials evoked by electrical stimulation of the olfactory nerve (Keller et al., 1998; Hsia et al., 1999; Aroniadou-Anderjaska et al., 2000; Ennis et al., 2001). Our results show that DA and GABA-B receptors are capable individually of suppressing odor-evoked sensory activity and resultant IOS. The additive effects of these two receptor systems were roughly linear, so that together they were capable of dramatically reducing the metabolic responses of the olfactory bulb to sensory stimulation. In addition to this, we also showed that blockade of GABA-B receptors increased odor-evoked IOS. To our knowledge, our data, together with reports from Wachowiak et al. (2005) and Vucinic et al. (2006), are some of

the first direct evidence that GABA-B receptors are activated by normal sensory-evoked activity in the olfactory bulb and that these receptors serve to limit transmission of sensory signals. We believe GABA-B and DA agonists to be acting presynaptically on ORN terminals because glomeruli express D2 and GABA-B receptors presynaptically (McLean and Shipley, 1988; Coronas et al., 1997; Duchamp-Viret et al., 1997; Bonino et al., 1999; Koster et al., 1999; Gutierrez-Mecinas et al., 2005). It remains possible that the small component that was not suppressed by these agonists reflects a release-independent component of the IOS (e.g., one due to some other mechanism of coupling of presynaptic action potentials). However, the data suggest that presynaptic action potentials are necessary, but not sufficient, to generate IOS.

Why is there a need for powerful and redundant feedback inhibition in the olfactory glomerulus? The high convergence ratio of ORNs to glomeruli (>5000:1, Mombaerts, 1999) and high probability of release from ORN terminals ($p \approx 1$; Murphy et al., 2004) imply that the glomerulus serves to amplify receptor signals by pooling input from many individual receptor neurons, perhaps facilitating odor detection. If a single mitral cell could be activated by a single receptor neuron at threshold odor concentrations, then higher concentrations of odorants would overwhelm the postsynaptic neurons well before saturating the olfactory receptors. Multiple presynaptic inhibitory feedback mechanisms could compress the dynamic range of the pooled sensory neuron input to that of M/TCs. The presence of astrocytes (Bailey and Shipley, 1993; Chao et al., 1997) containing glycogen (Coopersmith and Leon, 1995), intense glucose consumption (Johnson and Leon, 2000), and a dense capillary network (Chaigneau et al., 2003) are all signs of the high metabolic demands on processing in olfactory glomeruli. Our results demonstrate that presynaptic inhibition by GABA-B and DA receptors not only suppresses afferent neural activity (Nickell et al., 1994; Hsia et al., 1999; Wachowiak and Cohen, 1999; Aroniadou-Anderjaska et al., 2000; Berkowicz and Trombley, 2000; Ennis et al., 2001; Palouzier-Paulignan et al., 2002), but that GABA-B and DA receptors are highly effective in limiting the consumption of energy in the olfactory bulb (Sallaz and Jourdan, 1992). Presynaptic inhibition is likely to be critical in governing the interplay between maximization of information transmission and minimization of energy consumption.

Odor-evoked IOS were not blocked by antagonists of postsynaptic AMPA- and NMDA-type glutamate receptors (NBQX and DL-APV, respectively), while the same antagonists blocked electrically evoked LFPs. Thus, our data demonstrate that the generation of IOS does not depend on conventional synaptic transmission to activate postsynaptic electrical responses. Surprisingly, these antagonists actually increased odor-evoked IOS. One possible mechanism to explain this increase is the blockade of presynaptic inhibition mediated by JGCs (notably GABAergic JGCs) activated by glutamate released from ORN input terminals (Wachowiak et al., 2005; McGann et al., 2005; Vucinic et al., 2006). Consistent with this idea, the fractional increase in NBQX+APV was comparable to that produced by the GABA-B blocker SCH-50911 (around 20%).

The remaining glutamatergic pathway to the postsynaptic cell is through mGluR (van den Pol, 1995). mGluR1 agonists depolarize MCs (Schoppa and Westbrook, 1997) and induce Ca^{2+} transients in the apical dendrites of MCs (Yuan and Knopfel, 2006). However, the broad-spectrum group I/II mGluR antagonist MCPG and the specific mGluR1 antagonist LY367385 had no affect on odor-evoked signals. Thus, glomerular IOS do not appear to require any form of glutamatergic activation of M/TCs.

The lack of involvement of postsynaptic neurons in the generation of the IOS is counterintuitive insofar as postsynaptic signaling has been estimated to be the dominant cost term in the brain's energy budget (Attwell and Laughlin, 2001). However, our finding is consistent with conclusions from a study using two-photon imaging of blood flow in glomerular capillaries that showed that odor-evoked blood flow is not inhibited by glutamate receptor antagonists (E. Chaigneau, J. Lecoq, and S. Charpak, 2005, Soc. Neurosci. abstracts). Thus, both sensory-evoked IOS and blood flow appear to be independent of postsynaptic activation in olfactory glomeruli. Our findings are also in line with studies showing that odor-evoked IOS are well-correlated with presynaptic Ca^{2+} signals measured in ORN terminals (Wachowiak and Cohen, 2003).

The contribution of presynaptic versus postsynaptic activity to blood flow has been investigated in two other systems. The blood oxygenation level-dependent functional magnetic resonance imaging (BOLD-fMRI) signal in primary visual cortex of monkeys is better correlated with input and local activity than output (spiking) activity (Logothetis et al., 2001; Kayser et al., 2004), and stimulus-evoked changes in cerebral blood flow in the cerebellum depend on excitatory input but are independent of postsynaptic firing (Mathiesen et al., 1998; Caesar et al., 2003; Thomsen et al., 2004). Here we provide even more direct evidence that cutting off the postsynaptic electrical signaling pathway with glutamate antagonists does not interfere with the generation of sensory-evoked IOS.

Coupling Neural Activity to IOS through Astrocytic Glutamate Uptake

If IOS are not coupled to glutamate release through detection by postsynaptic neurons, then how is the glutamate signal transduced? Astrocytes are known to be central to numerous aspects of metabolic and synaptic signaling, including glutamate recycling and uptake and glucose metabolism, which are tightly linked (Pellerin and Magistretti, 1994; Cholet et al., 2001; Sibson et al., 1998; Voutsinos-Porche et al., 2003). Astrocytes are also key players in other metabolic processes such as extracellular potassium clearance (MacVicar and Hochman, 1991; MacVicar et al., 2002; Higashi et al., 2001; De Saint Jan and Westbrook, 2005), regulation of blood flow (Simard et al., 2003; Zonta et al., 2003; Mulligan and MacVicar, 2004; Takano et al., 2005), and shuttling of lactate to neurons (Pellerin and Magistretti, 1994; Bouzier-Sore et al., 2003). Astrocytic metabolic processing appears to be coupled to neural activity through multiple signaling pathways much as neurons are coupled to one another by multiple transmitters and receptors.

Odor-evoked IOS were inhibited by the GLAST and GLT1 blocker TBOA. This effect is consistent with the possibility that these astrocytic glutamate transporters themselves mediate the linkage between electrical and metabolic signals. However, TBOA also blocked, with variable efficacy, electrically recorded glomerular LFPs, an effect that could reflect a reduction of release by presynaptic mGluR activated by excess glutamate arising from blockade of transporters, as reported at some central synapses (Iserhot et al., 2004). Thus, we did not rule out the possibility that TBOA reduced odor-evoked IOS in part by reducing presynaptic release. Nevertheless, previous observations in olfactory glomeruli argue against this possibility. First, in vitro studies show that TBOA increases rather than decreases mitral cell activity (De Saint Jan and Westbrook, 2005). Second, TBOA has a relatively small effect on presynaptic ORN signals (McGann et al., 2005). Thus, it seems unlikely that the >60% block of IOS by TBOA can be explained by an indirect effect of presynaptic inhibition of transmitter release. Since postsynaptic neuronal responses were not required for generation of IOS, an astrocyte-mediated pathway is implied. Although the most obvious route is through the transporter itself, TBOA might also act indirectly by interfering with a glutamate sensor on astrocytes. Group I mGluR would be a chief candidate (e.g., Zonta et al., 2003; Wang et al., 2006), but the mGluR antagonist LY367385 did not alter the effect of TBOA when coapplied.

How Astrocytes Produce IOS

How could astrocyte activation lead to IOS? IOS are believed to arise from changes in three factors: light scattering, blood oxygenation level, and blood volume (Bonhoeffer and Grinvald, 1996). Previous work in the olfactory bulb suggested that glomerular IOS have a broad spectral profile consistent with light scattering (Meister and Bonhoeffer, 2001). In vitro studies have provided insight into how light-scattering changes are generated (Aitken et al., 1999). Glutamate uptake by GLT1 and GLAST relies on the electrochemical gradient of Na^+ ions as a driving force (Danbolt, 2001). The restoration of these gradients induces changes in osmolarity (MacAulay et al., 2004), causing cell swelling and a decrease in extracellular volume fraction that produces light-scattering changes (Fayuk et al., 2002). The relatively slow recovery of the IOS (tens of seconds) is consistent with the slow time scales of recovery from swelling (MacVicar et al., 2002) and astrocytic metabolic processing (Kasischke et al., 2004).

Direct measurements of capillary blood flow show that, in addition to the light-scattering change, sensory activity evokes a hemodynamic response in olfactory glomeruli (Chaigneau et al., 2003). These distinct sources reflect different aspects of metabolism and blood flow and, as discussed above, different signaling pathways. Group I mGluR (gluR1/5) activation is a pathway linking neuronal activity to the control of blood flow by astrocytes (Zonta et al., 2003), but blocking these mGluR had no affect on odor-evoked IOS. Therefore, either the contribution of blood flow signals to the IOS is minimal in our experiments, or else hemodynamic responses arise from a non-mGluR pathway in the olfactory glomeruli. The interplay between oxidative and nonoxidative metabolism (Fox and Raichle, 1986; Kasischke et al., 2004) will likely be a central determinant of the relative contributions of different metabolic signals to IOS. These contributions may depend on factors such as the type of neural tissue and the metabolic state of the animal (e.g., depth of anesthesia). The olfactory glomerulus is well-suited to further studies aimed at unraveling these relationships.

Metabolic Computation

In conclusion, the present data provide a novel view on the mechanisms entangling electrical and metabolic activity—information and energy—in the nervous system. It is increasingly recognized that energy consumption is a key constraint on neural function that must be considered alongside computational objectives (Attwell and Laughlin, 2001; Laughlin and Sejnowski, 2003). Our results demonstrate that functional metabolic signaling does not follow postsynaptic activation and energy consumption, but rather suggest a parallel arrangement that is likely to involve the direct activation of astrocytes by presynaptic glutamate release. This feedforward signaling pathway would place astrocytes in the role of not only responding to, but also predicting, energy demands of the postsynaptic neurons. Such an arrangement may seem overly complex, but it reflects the fact that energy supply and demand are not passively coupled: between the energy consumers (ion pumps, glutamate recycling, etc.) and the ultimate energy supply (glucose, oxygen) is an intricate metabolic network (Magistretti et al., 1999; Attwell and Iadecola, 2002; Raichle and Mintun, 2006). Astrocytes are clearly at the center of the complex problem of energy budgeting and calculation (Pellerin and Magistretti, 2004), and only by communicating rapidly and efficiently with neurons can they perform these functions. By detecting local glutamate release, astrocytes can not only perform direct support functions—recycling transmitter and maintaining ionic gradients—but also sense and participate in the metabolic computations of local circuits.

Experimental Procedures

Long Evans rats (200–300 g) were deeply anesthetized using medetomidine and fentanyl (0.05 and 0.01 mg/kg, i.p.) and placed in a stereotaxic frame. A local anesthetic (lidocaine) was applied topically during surgery. Anesthesia was maintained by periodic dosage with medetomidine (~0.25 mg/kg/hr). The bone over the dorsal surface of both olfactory bulbs was thinned using a dental drill and the bone and dura were carefully removed. Two small wells were constructed using dental cement around each hemi bulb. The wells were filled with agarose (2%) and covered with a glass coverslip to limit movements due to breathing. Body temperature was maintained at 37°C using a heating blanket throughout the experiment. Free breathing rate (~2 Hz) and partial oxygen pressure were monitored.

Data acquisition and analysis were performed using custom software (Z.F.M.) written in MATLAB (MathWorks, Natick, MA). Glomerular intrinsic signals were measured by the detection of red light reflectance using an analog CCD camera (Teli, Tokyo, Japan) mounted on a stereomicroscope (Olympus SZ40). Images were acquired at 30 Hz using a 10 bit frame grabber board (Matrox Pulsar, Dorval, Canada), temporally binned to 2 Hz, and saved to disk. The brain surface was illuminated using LEDs at 540 nm (for focusing 150 μm below pial surface) and LEDs at 630 or 660 nm (for imaging). Light reflectance values were collected over a 3 × 4 mm area (10 μm/pixel). Each imaging trial lasted 20 s, consisting of 5 s of

baseline, 10 s of odor presentation, and 5 s following stimulus termination (Figure 1A). Odors were delivered using a custom-designed, computer-controlled olfactometer (Uchida and Mainen, 2003) at intervals of 60 s.

IOS were quantified by calculating the relative change in reflectance, $\Delta R/R = (R_1 - R_0)/R_0$, where R_0 is the temporal average of images acquired 5 to 0 s before odor onset and R_1 is the average of images acquired 5 to 15 s after odor onset (Figure 1A). The $\Delta R/R$ images were separated into three components: the spatial average pixel value, $\Delta R/R_{avg}$; a low-pass filtered image, $\Delta R/R_{lp}$; and a high-pass filtered image, $\Delta R/R_{hp}$ (Figure 1B). To produce this decomposition, first $\Delta R/R_{avg}$ was calculated as the mean pixel value for each frame. By definition, $\Delta R/R_{avg}$ is spatially uniform; we also found this component to have a strong stimulus-independent temporal oscillation and to be TTX-independent (Figure 1). Next, $\Delta R/R_{lp}$ was calculated by convolving a Gaussian spatial kernel (σ = 200 μm) with the mean-subtracted image ($\Delta R/R - \Delta R/R_{avg}$). Subtracting these two components from the raw image yielded a high-pass filtered image: $\Delta R/R_{hp} = \Delta R/R - \Delta R/R_{lp} - \Delta R/R_{avg}$ (similar to Meister and Bonhoeffer, 2001). To calculate the time course of IOS signals (e.g., Figures 1C–1D), the average signal value was calculated within a region of interest (ROI) as a function of time (1 s resolution), and then $\Delta R/R$ was computed for each time point.

Drugs and agarose were dissolved in artificial cerebrospinal fluid containing, in mM, 127 NaCl, 25 $NaHCO_3$, 25 D-glucose, 2.5 KCl, 1.0 $MgCl_2$, 2.0 $CaCl_2$, and 1.25 NaH_2PO_4. Drugs were topically applied to one hemi-bulb by temporarily removing the coverslip and agarose. Gelfoam (Pharmacia and Upjohn, Kalamazoo, MI) containing drug-solution at 100 to 1000× slice concentration was applied on the surface of the olfactory bulb for 20 to 30 min. TTX, (RS)-baclofen, SCH-50911, DL-APV, NBQX, TBOA, MCPG, and LY367385 were purchased from Tocris (Avonmouth, UK), and R(–)apomorphine was purchased from Sigma-Aldrich (St. Louis, MO).

Overall experiment time was 6 to 7 hr, starting at anesthesia injection. IOS typically showed some amount of rundown during this time, as observed previously (Meister and Bonhoeffer, 2001). In a series of parallel experiments, we measured major blood parameters (blood gas analyzer Abl5, Radiometer Medical, Denmark) from the peripheral circulation to estimate the impact of anesthesia on physiological state over this period. Partial pressure of oxygen varied from 93.3 ± 2.3 to 82.0 ± 3.1 mm Hg (n = 3), partial pressure of carbon dioxide from 36.0 ± 2.6 to 43.3 ± 4.4 mm Hg (n = 3), pH from 7.3 ± 0.1 to 7.2 ± 0.1 (n = 3), and blood pressure from 106.7 ± 9.3 to 99.7 ± 5.8 mm Hg (n = 3). These results suggest that metabolic homeostasis is moderately affected by our anesthesia protocol and may be the cause of the rundown of IOS.

For each experiment, baseline-normalized amplitudes were calculated by dividing the average IOS amplitude ($\Delta R/R_{hp}$ unless otherwise noted) in an ROI by the average in the same ROI during pretreatment baseline trials (% baseline; Figures 2D, 3D, and 4D). Approximately symmetric ROIs were chosen for treated and control hemi-bulbs. Experiments were rejected if rundown exceeded 30%, but to compensate for the effect of any rundown on pharmacological treatments, cross-normalized amplitudes were calculated by dividing the baseline-normalized amplitude of the treated hemi-bulb after drug application by the baseline-normalized amplitude of the control hemi-bulb during the same time period (% control bulbs; Figure 2E and Figure 4E; Figure S1E). Statistical significance was calculated by comparing baseline-normalized control and treated bulb signals after drug application using a paired t test.

LFPs were recorded using either a glass pipette filled with 1–2 M NaCl (1–3 MΩ resistance) or a tungsten electrode (0.5 MΩ) lowered into the glomerular layer. A bipolar tungsten or stainless steal stimulating electrode was positioned on the surface of the olfactory bulb anterior and lateral to the recording site. Stimulus pulses (30 to 50 μA, 100 μs duration) were delivered at 0.1 Hz. Field potentials were recorded from a 70 to 150 μm depth and were band-pass filtered from 0.1 Hz to 10 kHz. Drugs were topically applied, and the electrical signals were acquired and analyzed using custom software (EXPER, Z.F.M.) running under MATLAB.

Supplemental Data

The Supplemental Data for this article can be found online at http://www.neuron.org/cgi/content/full/52/2/335/DC1/.

Acknowledgments

We thank Gilles Bonvento for comments on an earlier version of the text, and Markus Meister and Ed Soucy for helpful discussions and sharing unpublished data. This work was supported by the program "Imagerie du Petit Animal" of CNRS-CEA and the Cold Spring Harbor Laboratory Association (H.G.), by a fellowship from the Japan Society for the Promotion of Science and the Cold Spring Harbor Laboratory Association (N.U.), and by the NIDCD (5 R01 DC006104-03) as part of the NSF/NIH Collaborative Research in Computational Neuroscience Program (Z.F.M.).

Received: January 26, 2006
Revised: June 8, 2006
Accepted: July 25, 2006
Published: October 18, 2006

References

Aitken, P.G., Fayuk, D., Somjen, G.G., and Turner, D.A. (1999). Use of intrinsic optical signals to monitor physiological changes in brain tissue slices. Methods *18*, 91–103.

Araque, A., Carmignoto, G., and Haydon, P.G. (2001). Dynamic signaling between astrocytes and neurons. Annu. Rev. Physiol. *63*, 795–813.

Aroniadou-Anderjaska, V., Ennis, M., and Shipley, M.T. (1997). Glomerular synaptic responses to olfactory nerve input in rat olfactory bulb slices. Neuroscience *79*, 425–434.

Aroniadou-Anderjaska, V., Ennis, M., and Shipley, M.T. (1999). Dendrodendritic recurrent excitation in mitral cells of the rat olfactory bulb. J. Neurophysiol. *82*, 489–494.

Aroniadou-Anderjaska, V., Zhou, F.M., Priest, C.A., Ennis, M., and Shipley, M.T. (2000). Tonic and synaptically evoked presynaptic inhibition of sensory input to the rat olfactory bulb via GABA(B) heteroreceptors. J. Neurophysiol. *84*, 1194–1203.

Attwell, D., and Laughlin, S.B. (2001). An energy budget for signaling in the grey matter of the brain. J. Cereb. Blood Flow Metab. *21*, 1133–1145.

Attwell, D., and Iadecola, C. (2002). The neural basis of functional brain imaging signals. Trends Neurosci. *25*, 621–625.

Bailey, M.S., and Shipley, M.T. (1993). Astrocyte subtypes in the rat olfactory bulb: morphological heterogeneity and differential laminar distribution. J. Comp. Neurol. *328*, 501–526.

Belluscio, L., and Katz, L.C. (2001). Symmetry, stereotypy, and topography of odorant representations in mouse olfactory bulbs. J. Neurosci. *21*, 2113–2122.

Berkowicz, D.A., and Trombley, P.Q. (2000). Dopaminergic modulation at the olfactory nerve synapse. Brain Res. *855*, 90–99.

Berkowicz, D.A., Trombley, P.Q., and Shepherd, G.M. (1994). Evidence for glutamate as the olfactory receptor cell neurotransmitter. J. Neurophysiol. *71*, 2557–2561.

Bonhoeffer, T., and Grinvald, A. (1991). Iso-orientation domains in cat visual cortex are arranged in pinwheel-like patterns. Nature *353*, 429–431.

Bonhoeffer, T., and Grinvald, A. (1996). Optical imaging based on intrinsic signals: the methodology. In Brain Mapping: the Methods, A.W. Toga and J.C. Mazziotta, eds. (San Diego: Academic Press), pp. 55–97.

Bonino, M., Cantino, D., and Sassoe-Pognetto, M. (1999). Cellular and subcellular localization of gamma-aminobutyric acid B receptors in the rat olfactory bulb. Neurosci. Lett. *274*, 195–198.

Bonvento, G., Sibson, N., and Pellerin, L. (2002). Does glutamate image your thoughts? Trends Neurosci. *25*, 359–364.

Bouzier-Sore, A.K., Voisin, P., Canioni, P., Magistretti, P.J., and Pellerin, L. (2003). Lactate is a preferential oxidative energy substrate over glucose for neurons in culture. J. Cereb. Blood Flow Metab. *23*, 1298–1306.

Buchheim, K., Wessel, O., Siegmund, H., Schuchmann, S., and Meierkord, H. (2005). Processes and components participating in

the generation of intrinsic optical signal changes in vitro. Eur. J. Neurosci. *22*, 125–132.

Caesar, K., Gold, L., and Lauritzen, M. (2003). Context sensitivity of activity-dependent increases in cerebral blood flow. Proc. Natl. Acad. Sci. USA *100*, 4239–4244.

Chaigneau, E., Oheim, M., Audinat, E., and Charpak, S. (2003). Two-photon imaging of capillary blood flow in olfactory bulb glomeruli. Proc. Natl. Acad. Sci. USA *100*, 13081–13086.

Chao, T.I., Kasa, P., and Wolff, J.R. (1997). Distribution of astroglia in glomeruli of the rat main olfactory bulb: exclusion from the sensory subcompartment of neuropil. J. Comp. Neurol. *388*, 191–210.

Cholet, N., Pellerin, L., Welker, E., Lacombe, P., Seylaz, J., Magistretti, P., and Bonvento, G. (2001). Local injection of antisense oligonucleotides targeted to the glial glutamate transporter GLAST decreases the metabolic response to somatosensory activation. J. Cereb. Blood Flow Metab. *21*, 404–412.

Coopersmith, R., and Leon, M. (1995). Olfactory bulb glycogen metabolism: noradrenergic modulation in the young rat. Brain Res. *674*, 230–237.

Coronas, V., Srivastava, L.K., Liang, J.J., Jourdan, F., and Moyse, E. (1997). Identification and localization of dopamine receptor subtypes in rat olfactory mucosa and bulb: a combined in situ hybridization and ligand binding radioautographic approach. J. Chem. Neuroanat. *12*, 243–257.

De Saint Jan, D., and Westbrook, G.L. (2005). Detecting activity in olfactory bulb glomeruli with astrocyte recording. J. Neurosci. *25*, 2917–2924.

Danbolt, N.C. (2001). Glutamate uptake. Prog. Neurobiol. *65*, 1–105.

Duchamp-Viret, P., Coronas, V., Delaleu, J.C., Moyse, E., and Duchamp, A. (1997). Dopaminergic modulation of mitral cell activity in the frog olfactory bulb: a combined radioligand binding-electrophysiological study. Neuroscience *79*, 203–216.

Duchamp-Viret, P., Delaleu, J.C., and Duchamp, A. (2000). GABA(B)-mediated action in the frog olfactory bulb makes odor responses more salient. Neuroscience *97*, 771–777.

Ennis, M., Zimmer, L.A., and Shipley, M.T. (1996). Olfactory nerve stimulation activates rat mitral cells via NMDA and non-NMDA receptors in vitro. Neuroreport *7*, 989–992.

Ennis, M., Zhou, F.M., Ciombor, K.J., Aroniadou-Anderjaska, V., Hayar, A., Borrelli, E., Zimmer, L.A., Margolis, F., and Shipley, M.T. (2001). Dopamine D2 receptor-mediated presynaptic inhibition of olfactory nerve terminals. J. Neurophysiol. *86*, 2986–2997.

Ennis, M., Zhu, M., Heinbockel, T., and Hayar, A. (2006). Olfactory nerve-evoked, metabotropic glutamate receptor-mediated synaptic responses in rat olfactory bulb mitral cells. J. Neurophysiol. *95*, 2233–2241.

Fayuk, D., Aitken, P.G., Somjen, G.G., and Turner, D.A. (2002). Two different mechanisms underlie reversible, intrinsic optical signals in rat hippocampal slices. J. Neurophysiol. *87*, 1924–1937.

Fox, P.T., and Raichle, M.E. (1986). Focal physiological uncoupling of cerebral blood flow and oxidative metabolism during somatosensory stimulation in human subjects. Proc. Natl. Acad. Sci. USA *83*, 1140–1144.

Gall, C.M., Hendry, S.H., Seroogy, K.B., Jones, E.G., and Haycock, J.W. (1987). Evidence for coexistence of GABA and dopamine in neurons of the rat olfactory bulb. J. Comp. Neurol. *266*, 307–318.

Gutierrez-Mecinas, M., Crespo, C., Blasco-Ibanez, J.M., Gracia-Llanes, F.J., Marques-Mari, A.I., Nacher, J., Varea, E., and Martinez-Guijarro, F.J. (2005). Distribution of D2 dopamine receptor in the olfactory glomeruli of the rat olfactory bulb. Eur. J. Neurosci. *22*, 1357–1367.

Heeger, D.J., and Ress, D. (2002). What does fMRI tell us about neuronal activity? Nat. Rev. Neurosci. *3*, 142–151.

Heinbockel, T., Heyward, P., Conquet, F., and Ennis, M. (2004). Regulation of main olfactory bulb mitral cell excitability by metabotropic glutamate receptor mGluR1. J. Neurophysiol. *92*, 3085–3096.

Higashi, K., Fujita, A., Inanobe, A., Tanemoto, M., Doi, K., Kubo, T., and Kurachi, Y. (2001). An inwardly rectifying K(+) channel, Kir4.1, expressed in astrocytes surrounds synapses and blood vessels in brain. Am. J. Physiol. Cell Physiol. *281*, C922–C931.

Hsia, A.Y., Vincent, J.D., and Lledo, P.M. (1999). Dopamine depresses synaptic inputs into the olfactory bulb. J. Neurophysiol. *82*, 1082–1085.

Iserhot, C., Gebhardt, C., Schmitz, D., and Heinemann, U. (2004). Glutamate transporters and metabotropic receptors regulate excitatory neurotransmission in the medial entorhinal cortex of the rat. Brain Res. *1027*, 151–160.

Johnson, B.A., and Leon, M. (2000). Modular representations of odorants in the glomerular layer of the rat olfactory bulb and the effects of stimulus concentration. J. Comp. Neurol. *422*, 496–509.

Kasischke, K.A., Vishwasrao, H.D., Fisher, P.J., Zipfel, W.R., and Webb, W.W. (2004). Neural activity triggers neuronal oxidative metabolism followed by astrocytic glycolysis. Science *305*, 99–103.

Kayser, C., Kim, M., Ugurbil, K., Kim, D.S., and Konig, P. (2004). A comparison of hemodynamic and neural responses in cat visual cortex using complex stimuli. Cereb. Cortex *14*, 881–891.

Keller, A., Yagodin, S., Aroniadou-Anderjaska, V., Zimmer, L.A., Ennis, M., Sheppard, N.F., Jr., and Shipley, M.T. (1998). Functional organization of rat olfactory bulb glomeruli revealed by optical imaging. J. Neurosci. *18*, 2602–2612.

Kleinfeld, D., Mitra, P.P., Helmchen, F., and Denk, W. (1998). Fluctuations and stimulus-induced changes in blood flow observed in individual capillaries in layers 2 through 4 of rat neocortex. Proc. Natl. Acad. Sci. USA *95*, 15741–15746.

Koster, N.L., Norman, A.B., Richtand, N.M., Nickell, W.T., Puche, A.C., Pixley, S.K., and Shipley, M.T. (1999). Olfactory receptor neurons express D2 dopamine receptors. J. Comp. Neurol. *411*, 666–673.

Laughlin, S.B., and Sejnowski, T.J. (2003). Communication in neuronal networks. Science *301*, 1870–1874.

Logothetis, N.K., Pauls, J., Augath, M., Trinath, T., and Oeltermann, A. (2001). Neurophysiological investigation of the basis of the fMRI signal. Nature *412*, 150–157.

MacAulay, N., Hamann, S., and Zeuthen, T. (2004). Water transport in the brain: role of cotransporters. Neuroscience *129*, 1031–1044.

MacVicar, B.A., and Hochman, D. (1991). Imaging of synaptically evoked intrinsic optical signals in hippocampal slices. J. Neurosci. *11*, 1458–1469.

MacVicar, B.A., Feighan, D., Brown, A., and Ransom, B. (2002). Intrinsic optical signals in the rat optic nerve: role for K(+) uptake via NKCC1 and swelling of astrocytes. Glia *37*, 114–123.

Magistretti, P.J., Pellerin, L., Rothman, D.L., and Shulman, R.G. (1999). Energy on demand. Science *283*, 496–497.

Mathiesen, C., Caesar, K., Akgoren, N., and Lauritzen, M. (1998). Modification of activity-dependent increases of cerebral blood flow by excitatory synaptic activity and spikes in rat cerebellar cortex. J. Physiol. *512*, 555–566.

Mayhew, J.E., Askew, S., Zheng, Y., Porrill, J., Westby, G.W., Redgrave, P., Rector, D.M., and Harper, R.M. (1996). Cerebral vasomotion: a 0.1-Hz oscillation in reflected light imaging of neural activity. Neuroimage *4*, 183–193.

McGann, J.P., Pirez, N., Gainey, M.A., Muratore, C., Elias, A.S., and Wachowiak, M. (2005). Odorant representations are modulated by intra- but not interglomerular presynaptic inhibition of olfactory sensory neurons. Neuron *48*, 1039–1053.

McLean, J.H., and Shipley, M.T. (1988). Postmitotic, postmigrational expression of tyrosine hydroxylase in olfactory bulb dopaminergic neurons. J. Neurosci. *8*, 3658–3669.

Meister, M., and Bonhoeffer, T. (2001). Tuning and topography in an odor map on the rat olfactory bulb. J. Neurosci. *21*, 1351–1360.

Mombaerts, P. (1999). Seven-transmembrane proteins as odorant and chemosensory receptors. Science *286*, 707–711.

Mulligan, S.J., and MacVicar, B.A. (2004). Calcium transients in astrocyte endfeet cause cerebrovascular constrictions. Nature *431*, 195–199.

Murphy, G.J., Glickfeld, L.L., Balsen, Z., and Isaacson, J.S. (2004). Sensory neuron signaling to the brain: properties of transmitter release from olfactory nerve terminals. J. Neurosci. *24*, 3023–3030.

Nedergaard, M., Ransom, B., and Goldman, S.A. (2003). New roles for astrocytes: redefining the functional architecture of the brain. Trends Neurosci. *26*, 523–530.

Nickell, W.T., Behbehani, M.M., and Shipley, M.T. (1994). Evidence for GABAB-mediated inhibition of transmission from the olfactory nerve to mitral cells in the rat olfactory bulb. Brain Res. Bull. *35*, 119–123.

Ogawa, S., Lee, T.M., Kay, A.R., and Tank, D.W. (1990). Brain magnetic resonance imaging with contrast dependent on blood oxygenation. Proc. Natl. Acad. Sci. USA *87*, 9868–9872.

Palouzier-Paulignan, B., Duchamp-Viret, P., Hardy, A.B., and Duchamp, A. (2002). GABA(B) receptor-mediated inhibition of mitral/tufted cell activity in the rat olfactory bulb: a whole-cell patch-clamp study in vitro. Neuroscience *111*, 241–250.

Pellerin, L., and Magistretti, P.J. (1994). Glutamate uptake into astrocytes stimulates aerobic glycolysis: a mechanism coupling neuronal activity to glucose utilization. Proc. Natl. Acad. Sci. USA *91*, 10625–10629.

Pellerin, L., and Magistretti, P.J. (2004). Neuroenergetics: calling upon astrocytes to satisfy hungry neurons. Neuroscientist *10*, 53–62.

Raichle, M.E. (2003). Functional brain imaging and human brain function. J. Neurosci. *23*, 3959–3962.

Raichle, M.E., and Mintun, M.A. (2006). Brain work and brain imaging. Annu. Rev. Neurosci. *29*, 449–476.

Rubin, B.D., and Katz, L.C. (1999). Optical imaging of odorant representations in the mammalian olfactory bulb. Neuron *23*, 499–511.

Sallaz, M., and Jourdan, F. (1992). Apomorphine disrupts odour-induced patterns of glomerular activation in the olfactory bulb. Neuroreport *3*, 833–836.

Schneider, G.H., Baethmann, A., and Kempski, O. (1992). Mechanisms of glial swelling induced by glutamate. Can. J. Physiol. Pharmacol. Suppl. *70*, S334–S343.

Schoppa, N.E., and Westbrook, G.L. (1997). Modulation of mEPSCs in olfactory bulb mitral cells by metabotropic glutamate receptors. J. Neurophysiol. *78*, 1468–1475.

Schoppa, N.E., and Westbrook, G.L. (2001). Glomerulus-specific synchronization of mitral cells in the olfactory bulb. Neuron *31*, 639–651.

Shepherd, G.M., and Greer, C.A. (1998). The olfactory bulb. In The Synaptic Organization of the Brain, Fourth Edition, G.M. Shepherd, ed. (New York: Oxford University Press), pp. 159–203.

Shulman, R.G., and Rothman, D.L. (1998). Interpreting functional imaging studies in terms of neurotransmitter cycling. Proc. Natl. Acad. Sci. USA *95*, 11993–11998.

Sibson, N.R., Dhankhar, A., Mason, G.F., Rothman, D.L., Behar, K.L., and Shulman, R.G. (1998). Stoichiometric coupling of brain glucose metabolism and glutamatergic neuronal activity. Proc. Natl. Acad. Sci. USA *95*, 316–321.

Simard, M., Arcuino, G., Takano, T., Liu, Q.S., and Nedergaard, M. (2003). Signaling at the gliovascular interface. J. Neurosci. *23*, 9254–9262.

Takano, T., Tian, G.F., Peng, W., Lou, N., Libionka, W., Han, X., and Nedergaard, M. (2005). Astrocyte-mediated control of cerebral blood flow. Nat. Neurosci. *9*, 260–267.

Thomsen, K., Offenhauser, N., and Lauritzen, M. (2004). Principal neuron spiking: neither necessary nor sufficient for cerebral blood flow in rat cerebellum. J. Physiol. *560*, 181–189.

Uchida, N., and Mainen, Z.F. (2003). Speed and accuracy of olfactory discrimination in the rat. Nat. Neurosci. *6*, 1224–1229.

Uchida, N., Takahashi, Y.K., Tanifuji, M., and Mori, K. (2000). Odor maps in the mammalian olfactory bulb: domain organization and odorant structural features. Nat. Neurosci. *3*, 1035–1043.

Utsumi, M., Ohno, K., Onchi, H., Sato, K., and Tohyama, M. (2001). Differential expression patterns of three glutamate transporters (GLAST, GLT1 and EAAC1) in the rat main olfactory bulb. Brain Res. Mol. Brain Res. *92*, 1–11.

van den Pol, A.N. (1995). Presynaptic metabotropic glutamate receptors in adult and developing neurons: autoexcitation in the olfactory bulb. J. Comp. Neurol. *359*, 253–271.

Voutsinos-Porche, B., Knott, G., Tanaka, K., Quairiaux, C., Welker, E., and Bonvento, G. (2003). Glial glutamate transporters and maturation of the mouse somatosensory cortex. Cereb. Cortex *13*, 1110–1121.

Vucinic, D., Cohen, L.B., and Kosmidis, E.K. (2006). Interglomerular center-surround inhibition shapes odorant-evoked input to the mouse olfactory bulb in vivo. J. Neurophysiol. *95*, 1881–1887.

Wachowiak, M., and Cohen, L.B. (1999). Presynaptic inhibition of primary olfactory afferents mediated by different mechanisms in lobster and turtle. J. Neurosci. *19*, 8808–8817.

Wachowiak, M., and Cohen, L.B. (2003). Correspondence between odorant-evoked patterns of receptor neuron input and intrinsic optical signals in the mouse olfactory bulb. J. Neurophysiol. *89*, 1623–1639.

Wachowiak, M., Denk, W., and Friedrich, R.W. (2004). Functional organization of sensory input to the olfactory bulb glomerulus analyzed by two-photon calcium imaging. Proc. Natl. Acad. Sci. USA *101*, 9097–9102.

Wachowiak, M., McGann, J.P., Heyward, P.M., Shao, Z., Puche, A.C., and Shipley, M.T. (2005). Inhibition of olfactory receptor neuron input to olfactory bulb glomeruli mediated by suppression of presynaptic calcium influx. J. Neurophysiol. *94*, 2700–2712.

Wang, X., Lou, N., Xu, Q., Tian, G.F., Peng, W.G., Han, X., Kang, J., Takano, T., and Nedergaard, M. (2006). Astrocytic Ca(2+) signaling evoked by sensory stimulation in vivo. Nat. Neurosci. *9*, 816–823.

Yuan, Q., and Knopfel, T. (2006). Olfactory nerve stimulation-evoked mGluR1 slow potentials, oscillations, and calcium signaling in mouse olfactory bulb mitral cells. J. Neurophysiol. *95*, 3097–3104.

Zonta, M., Angulo, M.C., Gobbo, S., Rosengarten, B., Hossmann, K.A., Pozzan, T., and Carmignoto, G. (2003). Neuron-to-astrocyte signaling is central to the dynamic control of brain microcirculation. Nat. Neurosci. *6*, 43–50.